Article

Stereodynamics Study of the Reaction of O(^{3}P) with CH$_4$ (v = 0,j = 0)

Yufang Liu *, Yali Gao, Hongsheng Zhai, Deheng Shi and Jinfeng Sun

Department of Physics, Henan Normal University, Xinxiang 453007, China;
E-Mails: hongsheng419@163.com (H.Z.); scattering@sina.com (D.S.);
wlxyzfz@henannu.edu.cn (J.S.)

* Author to whom correspondence should be addressed; E-Mail: yf-liu@henannu.edu.cn;
Tel. +86-373-3329097; Fax: +86-373-3326187

Abstract: A new London-Eyring-Polanyi-Sato (LEPS) potential energy surface (PES) is used in the O + CH$_4$ → OH + CH$_3$ reaction via the quasiclassical trajectory method (QCT). Comparing with the experiments and the former *ab initio* calculations, the new LEPS PES describes the actual potential energy surface of the O + CH$_4$ reaction successfully. The four polarization dependent "generalized" differential cross sections (PDDCS) are presented in the center of mass frame. In the meantime, the distribution of dihedral angle [$P(\phi_r)$, the distribution of angle between k and j' ($P(\theta_r)$)] and the angular distribution of product rotational vectors in the form of polar plots in θ_r and ϕ_r (P(θ_r, ϕ_r) are calculated. The isotope effect for the reactions O + CD$_4$ is also calculated. These results are in good agreement with the experiments.

Keywords: quasiclassical trajectory; potential barrier; polarization; isotope effect

1. Introduction

The reactions of ground-state atomic oxygen, O(^{3}P), with hydrocarbons are the important initial steps of oxidation in combustion processes [1] and in Low Earth Orbit (LEO) conditions [2]. Among those reactions, the abstraction reaction O(^{3}P) + CH$_4$ → OH + CH$_3$ has attracted considerable interest, both in experimental [3-7,11] and theoretical [8-10,12-20] calculations over the past decades. The rate constant values have been established in experiments [3,4]. Experimental studies have reported the

translational energy release to the umbrella mode of the CH_3 product [5] as well as OH ro-vibrational distributions [6,7]. The thermal rate constants have been measured with a wide variety of methods [8-10]. The state distribution of the OH product was found by experiments [5,6,8,11] and theoretical [12] calculations. A small amount of OH rotational excitation was found [5,6,11], which has been interpreted as resulting from a direct abstraction mechanism with a preferentially collinear O-H-C approach of the $O(^3P)$ atom attacking to the C-H bond. Theoretical calculations [8,9,12,13] showed that this reaction has a collinear $O-H-CH_3$ transition state. The classical barrier height is around 0.4 eV [20,21]. Reduced-dimensionality quantum [16-19] models have been reported. The calculated kinetic behaviors and product state distributions are generally in good agreement with experimental findings [7].

It has been recognized that the correlated angular distribution provides an informative three-dimensional picture of a chemical reaction [22-25]. The angular distribution of the reagent and product relative velocity vector (k, k') is characterized by the differential cross-section $d\,\sigma/d\,\omega_t$. Furthermore, the angular distribution describing the relative orientation of vectors k, k' and product rotational quantum number j' in space may be termed the k - k' - j' distribution. The correlations among three vectors in the center-of-mass frame can be characterized by certain interesting double and triple vector correlations [26]. To our best knowledge, there is only one experimental work [27] relate to the product angular distribution (k - k'), scalar and two-vector properties of the reaction were analyzed using the QCT method [14], the full-dimensional trajectory [13,20] calculations only relate to the k - k' angular distributions. So the full product angular distribution of this reaction has not been reported.

We calculated the product rotational polarization, the scattering-angle resolved product rotational alignment, the vector correlations of the reaction $O(^3P) + CH_4 \rightarrow OH + CH_3$ and the isotope effect for the reactions $O + CH_4/O + CD_4$.

2. Results and Discussion

Figure 1 shows the minimum energy paths of the reaction $O + CH_4 \rightarrow OH + CH_3$ at the collision energy of 0.65 eV from reactants to products on our chosen PESs. A new LEPS PES with a different set of Sato parameters has been calculated in our work. The Sato C parameters from [33] are on the PES1 and the Sato D parameters which we calculated are on the PES2. We get the Sato D parameters from the *ab initio* calculation carried out by Troya and García-Molina [20] when the quality of the minimum energy path on the new LEPS potential energy surface accords with the experimental results. In Figure 1, there is a potential barrier in the reaction. The values of the potential barrier are 11 kcal/mol on PES1 and 9.23 kcal/mol on PES2. The results on PES2 are accord with the calculation [20] in which the barrier is around 9.22 kal/mol. The product's ro-vibrational distributions are shown in Figure 2. From Figure 2(a) we can see that the most probable vibrational quantum number of OH is $v' = 0$. In Figure 2(b) the most probable rotational quantum number of OH is $j' = 1$, which is quite close to the calculation [20] and experiment [37], but the product OH of our calculation is colder than the experimental results. The reason is that the collision energy changes to the product's translational energy rather than rotational energy in the $O+CH_4$ direct abstraction reaction.

Figure 1. The reaction profile along the minimum energy paths of the O + CH$_4$ reaction on the PES1 and PES2.
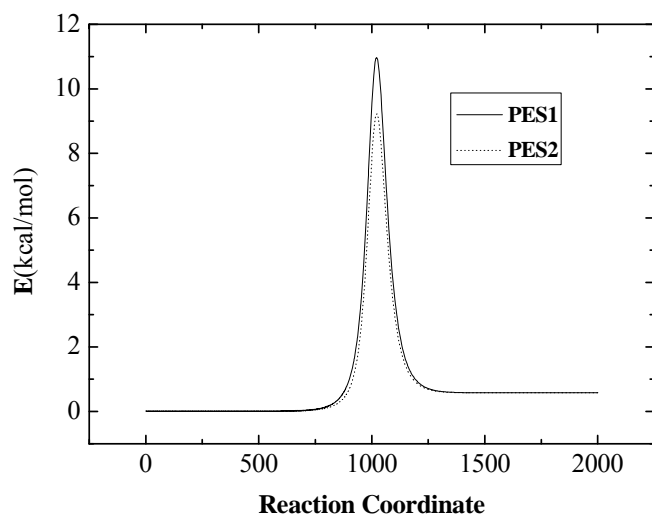

Figure 2. (a) The vibrational population of the product OH. (b) The rotational population of the products OH. The solid square symbol is our results, the circle symbol is experimental data, and the triangle symbol is taken from [20]. (c) The DCS distribution of the product OH at collision energy 0.54 eV. The solid line is the result on the PES2, the dash line is the result on the PES1 and the dot line is the experimental results. (d) The DCS distribution of the product OH at collision energy 0.65 eV. The solid line is our result, the solid line and solid square symbol are taken from [16], the solid line and solid triangle symbol are taken from [20].
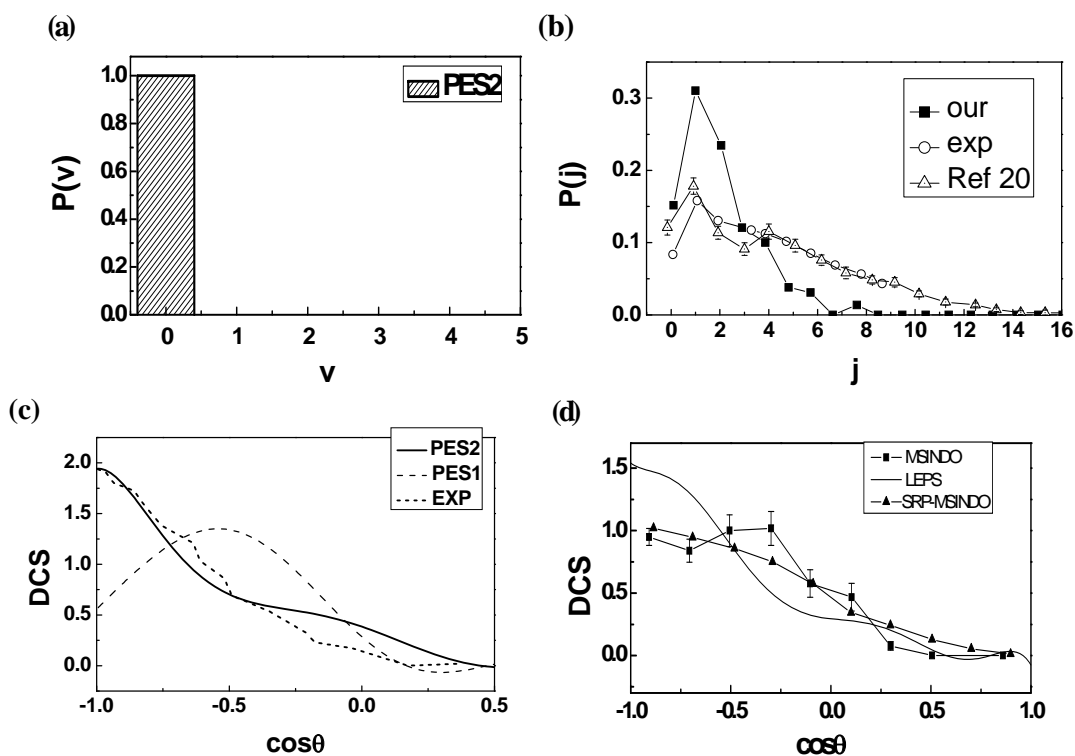
In the direct abstraction reaction, the rotational distribution is always in the narrow and low range of the rotational energy. The PDDCS $(2\pi/\sigma)(d\sigma_{00}/d\omega_t)$, which is proportional to the differential cross section (DCS), predicts the angular distribution of the product molecular. In Figures 2(c,d) the DCS distribution is quite close to the experiment [27] and calculations [13,20]. The PES2 reflecting the real reaction process is much better than the PES1.

The value of $(2\pi/\sigma)(d\sigma_{20}/d\omega_t)$, which is the expectation value of the second Legendre moment, shows the trend which is opposite to that of $(2\pi/\sigma)(d\sigma_{00}/d\omega_t)$. At the extremes of forward and backward scattering, the PDDCSs with q $\neq$ 0 are necessarily zero. At these limiting scattering angles, the k -k' scattering plane is not determined and the value of these PDDCSs with q $\neq$ 0 must be zero. The variations of the PDDCSs with k = 2 reflect changes in the rotational polarization with the scattering angles and suggest that the PDDCSs for the O+CH4 reaction contain important dynamical information. The four PDDCS of the OH product state are shown in Figure 3(a).

Figure 3. The collision energy is 0.65eV (a) Four PDDCS, boldfaced solid line indicating $(2\pi/\sigma)(d\sigma_{00}/d\omega_t)$, thin solid line indicating $(2\pi/\sigma)(d\sigma_{20}/d\omega_t)$, dash dot indicating $(2\pi/\sigma)(d\sigma_{22+}/d\omega_t)$ and short dot indicating $(2\pi/\sigma)(d\sigma_{21-}/d\omega_t)$.(b) The distribution of $P(\theta_r)$, reflecting the k - J' correlation.(c) The dihedral angle distribution of J', $P(\varphi_r)$ with respect to the k -k' plane.(d) Polar plots of $P(\theta_r,\ \phi_r)$ distribution averaged over all scattering angles.
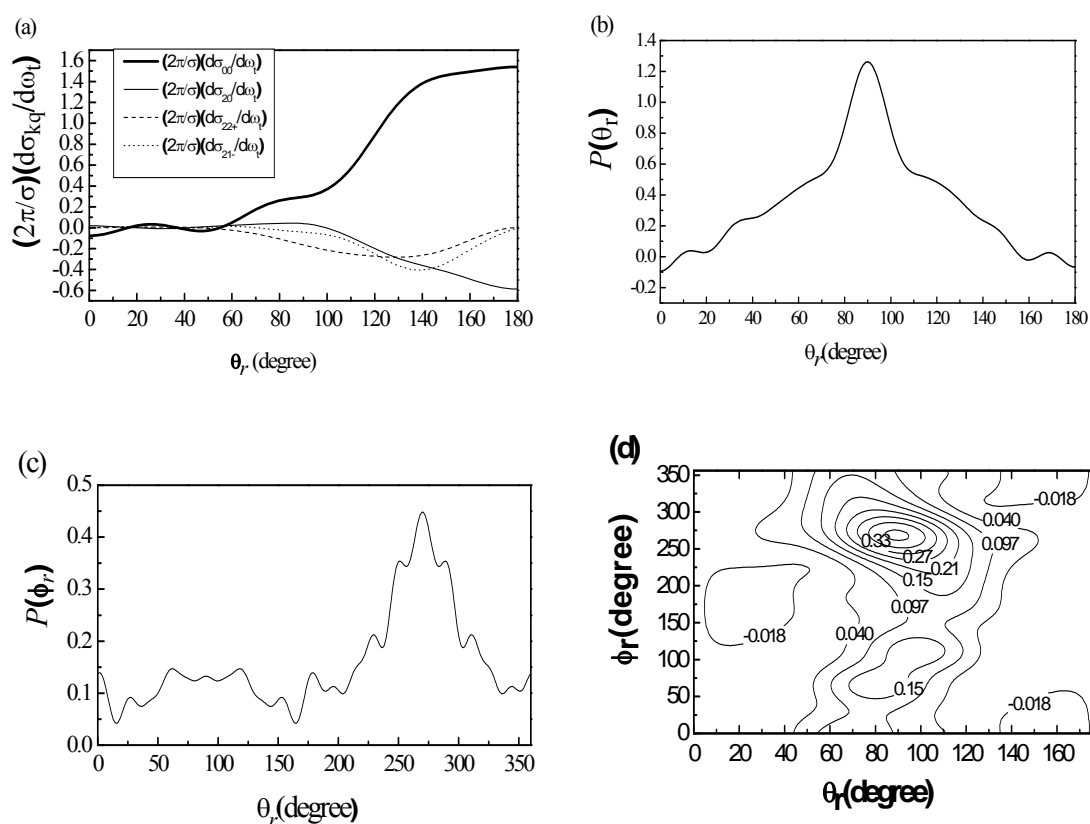
It indicates that the product OH scatters backward. The angular distribution that is asymmetric with $\theta_r = 90°$ is characteristic of a direct reaction mechanism. The available energy is released as product

translation energy rather than internal excitation, and the product internal excitation is quite cold. This is consistent with Figure 2.

The $P(\theta_r)$ and $P(\phi_r)$ distributions are shown in Figures 3(b,c). We can get better graphical representation of the products polarization for the reaction O + CH$_4$. Figure 3(b) clearly shows that the distributions of the k - j' correlation P(θ_r) peak at θ_r angle close to $\theta_r = 90°$ and is symmetric with $\theta_r = 90°$. It demonstrates that j_{OH} is strongly aligned perpendicular to the line of centers. The distribution of the k - k' - j' correlation $P(\phi_r)$ is shown in Figure 3(c). The $P(\phi_r)$ tends to be asymmetric about $\phi_r = 180°$, reflecting the strong polarization of angular momentum. There are two peaks of $P(\phi_r)$, respectively $\phi_r = 270°$ and $\phi_r = 90°$. It implies that the angular momentum (j_{OH}) of the most product molecules aligns along the CM y-axis. This behavior suggests that the reaction proceeds preferentially when the reactant velocity vector lies in the plane containing all three atoms. However, for an initially random orientation of reactant molecules the probability of such planar collisions is very low; thus, we can conclude that the given PES reorients or polarizes the plane containing the three atoms into the k - k' plane during the reaction process. The distribution of $P(\theta_r, \phi_r)$ is presented in Figure 3(d); one peak appears at (*90°, 270°*). This suggests that the OH products are preferentially polarized perpendicular to the k - k' plane. The $P(\theta_r, \phi_r)$ distribution is not symmetric about $\phi_r=180°$, reflecting the nonzero values of the PDDCS *(2π/σ)(dσ₀₀/dω$_t$)* for the O + CH4 reaction. It is in good accordance with the distribution of $P(\phi_r)$ that the dihedral angle distribution tends to be asymmetric with respect to the scattering plane.

Figure 4(a) presents the PDDCSs *(2π/σ)(dσ₀₀/dω$_t$)* distributions of the products OH and OD at the collision energy of 0.65eV. The distribution of the products OD is a little more backward than that of the products OH. The increase of backward scattering with the mass number indicates that the rotational angular momenta distribution of the products is sensitive to the factor of merit [the factor of merit is $\cos^2\beta = m_A m_C/(m_A + m_B)(m_B + m_C)$ for the reaction A + BC → AB + C] [32,34].

The product polarization distributions for the reaction O + CH$_4$ and O + CD$_4$ are shown in Figures 4(b,c) that describe the visible stereodynamics isotope effect. Figure 4(b) illustrates that the product distribution of *P(θ$_r$)* for the O+ CD$_4$ reaction is a little broader than that for O + CH$_4$ reaction. This means that the rotational orientation effect of the product becomes weaker with the increase of the atomic mass. Han *et al.* [32,34]. have studied the product polarization for the reaction *H + H'L* (H, heavy; L, light), they found that the distribution of the product rotational angular momentum vectors is acutely sensitive to the mass factor, furthermore the increase of the mass factor can reduce the anisotropic distribution of the angular momentum *j'* of the product molecule. The effect of mass factor $\cos^2\beta = m_A m_C/(m_A + m_B)(m_B + m_C)$ on product rotational alignment is notable for the HHL mass combination reaction. The mass factor of the O + CD$_4$ reaction is larger than that of the O + CH$_4$ reaction. So the *j'* tend toward a less anisotropic distribution with respect to the vector k, while the rotation of the product from the O + CH$_4$ is strongly aligned. During the reactive encounter, total angular momentum is conserved, *j + L = j' + L'* (here L and *L'* are the reagent and product orbital angular momenta). According to the impulse model and $j' = L\sin^2\beta + j\cos^2\beta + J_1 m_B/m_{AB}$, the larger product atom will take more angular momentum away, so the increase of the mass factor reduces the anisotropic distribution of *j'*.

Figure 4. The collision energy is 0.65eV (a) The distribution of $(2\pi/\sigma)(d\sigma_{00}/d\omega_t)$, reflecting the $k-k'$ correlation for O + CH$_4$ and O + CD$_4$ on the PES2. (b) The distribution of $P(\theta_r)$, reflecting the k - j' correlation for O + CH$_4$ and O + CD$_4$ on the PES2. (c) The distribution of $P(\phi_r)$, reflecting the k - k' - j' correlation for O + CH$_4$ and O + CD$_4$ on the PES2. Solid line indicating the reaction O + CH$_4$, and short dot indicating the reaction O + CD$_4$.
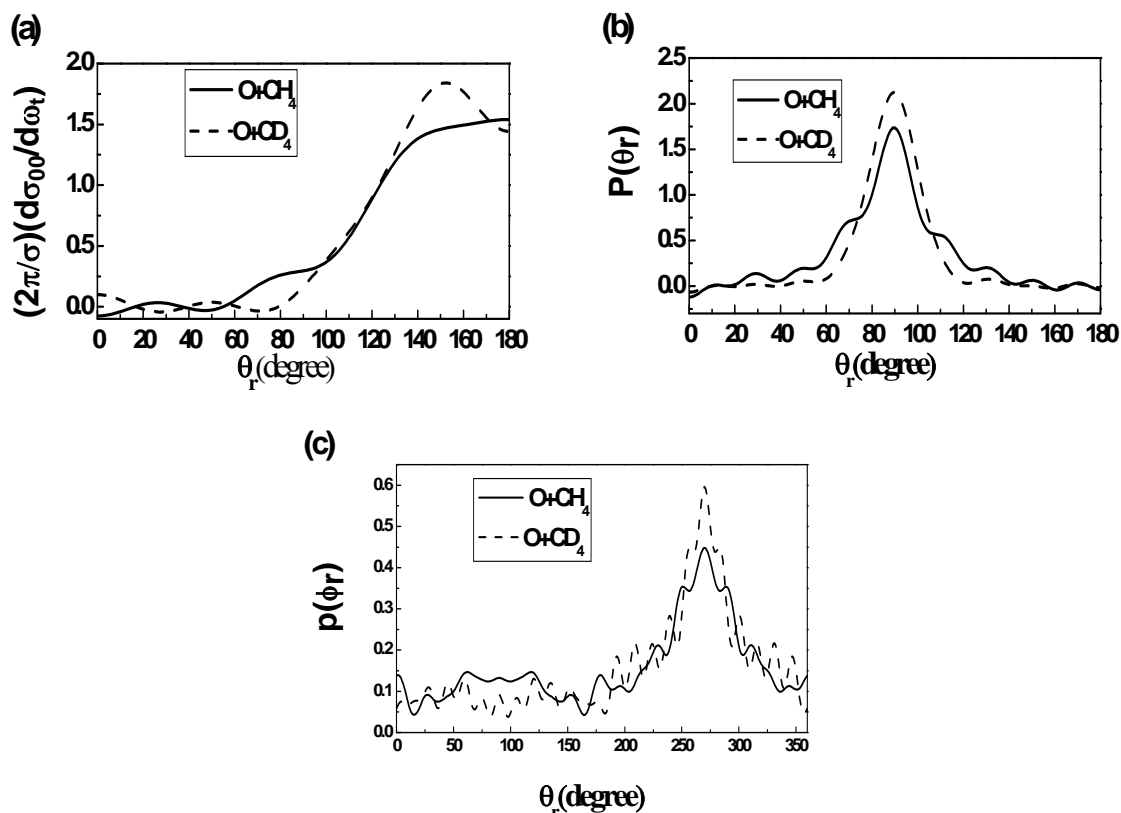

Figure 4(c) describes that the $P(\phi_r)$ distribution becomes a little broader when the H atoms are displaced by the D atoms. With the increase of the atomic mass, the preference for in-plane reaction c gradually hanges to a preference for an out-of-plane mechanism. The mass effect causes the reaction O + CD4 to prefer an out-of-plane mechanism. That is to say, it is not necessary that the product molecules rotate in the scattering plane containing all the three atoms when the reaction occurs. According to the [35] and [36], the $P(\phi_r)$ is relevant to PES and the mass factor. We consider that the difference of the $P(\phi_r)$ distribution is probably attributed to the different mass number and to the isotope effect. The obvious variation in the dihedral distribution implies that the mass effect plays an important role in the dynamical stereochemistry.

3. Experimental Section

3.1. Product rotational polarization in the center-of-mass (CM) frame

The center-of-mass (CM) frame is chosen; in this frame, the z-axis is parallel to the reagent relative velocity k, and the y-axis is perpendicular to the xz-plane which contains k and k'. The distribution of the angular momentum j' of the product molecule is described by the function $f(\theta_r)$, where θ_r is the angle between j' and k. $f(\theta)$ can be represented by Legendre polynomial [26]:

$$f(\theta_r) = \sum a_n p_n(\cos \theta_r) \tag{1}$$

n = 2 indicates the product rotational alignment $\langle p_2(j' \cdot k)\rangle = \langle 3\cos^2\theta_r - 1\rangle/2$, where p_2 is the second Legendre moment, and the brackets indicate an average over the distribution of j' about k.

The full three-dimensional angular distribution associated with k, k' and j' can be represented by a set of generalized polarization-dependent differential cross-sections (PDDCSs) in the CM frame. The k - k' - j' correlated CM angular distribution is written as the sum [26,29].

$$p(\omega_t, \omega_r) = \sum_{kq} \frac{[k]}{4\pi} \frac{1}{\sigma} \frac{d\sigma_{kq}}{d\omega_t} C_{kq}(\theta_r, \phi_r)^* \tag{2}$$

where $(1/\sigma)(d\sigma_{kq}/d\omega_t)$ is a generalized polarization-dependent differential cross-section (PDDCS), and $(1/\sigma)(d\sigma_{kq}/d\omega_t)$ yields.

$$\frac{1}{\sigma} \frac{d\sigma_{k0}}{d\omega_t} = 0 \qquad\qquad k \text{ is odd,} \tag{3}$$

$$\frac{1}{\sigma} \frac{d\sigma_{kq+}}{d\omega_t} = \frac{1}{\sigma} \frac{d\sigma_{kq}}{d\omega_t} + \frac{1}{\sigma} \frac{d\sigma_{k-q}}{d\omega_t} = 0, \ k \text{ is even, } q \text{ is odd or } k \text{ is odd, } q \text{ is even.,} \tag{4}$$

$$\frac{1}{\sigma} \frac{d\sigma_{kq-}}{d\omega_t} = \frac{1}{\sigma} \frac{d\sigma_{kq}}{d\omega_t} - \frac{1}{\sigma} \frac{d\sigma_{k-q}}{d\omega_t} = 0, \ k \text{ is even, } q \text{ is even or } k \text{ is odd, } q \text{ is odd.} \tag{5}$$

The PDDCS is written in the following form:

$$\frac{1}{\sigma} \frac{d\sigma_{kq\pm}}{d\omega_t} = \frac{1}{4\pi} \sum_{k_1} [k_1] S^{k_1}_{kq\pm} C_{k_1-q}(\theta_t, 0) \tag{6}$$

where the $S^{k_1}_{kq\pm}$ is evaluated using the expected value expression

$$S^{k_1}_{kq\pm} = \left\langle C_{k_1 q}(\theta_t, 0) C_{kq}(\theta_r, 0)[(-1)^q e^{iq\varphi_r} \pm e^{-iq\varphi_r}]\right\rangle \tag{7}$$

where the angular brackets represent an average over all angles.

The PDDCS with q=0 is presented by:

$$\frac{1}{\sigma} \frac{d\sigma_{k0}}{d\omega_t} = \frac{1}{4\pi} \sum_{k_1} [k_1] S^{k_1}_{k0} p_{k_1}(\cos \theta_t) \tag{9}$$

where $S_{k0}^{k_1}$ is evaluated by the expected value expression:

$$S_{k0}^{k_1} = \langle p_{k_1}(\cos\theta_t) p_k(\cos\theta_r) \rangle \tag{10}$$

The differential cross-section is given by:

$$\frac{1}{\sigma}\frac{d\sigma_{00}}{d\omega_t} \equiv p(\omega_t) = \frac{1}{4\pi}\sum_{k_1}[k_1]h_0^{k_1}(k_1,0) p_{k_1}(\cos\theta_t) \tag{11}$$

the bipolar moments $h_0^{k_1}(k_1,0)$ are evaluated using the expectation values of the Legendre moments of the differential cross-section: $S_{00}^{k_1} = h_0^{k_1}(k_1,0) = \langle p_k(\cos\theta_t) \rangle$.

In many photoinitiated bimolecular reaction experiments, we will be sensitive to only those polarization moments with $k = 0$ and $k = 2$. In order to compare calculations with experiments, $(2\pi/\sigma)(d\sigma_{00}/d\omega_t)$, $(2\pi/\sigma)(d\sigma_{20}/d\omega_t)$, $(2\pi/\sigma)(d\sigma_{22+}/d\omega_t)$ and $(2\pi/\sigma)(d\sigma_{21 -}/d\omega_t)$ are calculated. In the computation, PDDCSs are expanded up to k_1=7, which is sufficient for good convergence.

The usual two vector correlations (k - k', k - j', k' - j') are expanded in a series of Legendre polynomials. The distribution of the k - j' correlation is characterized by $P(\theta_r)$ and the $P(\theta_r)$ can be written as [26-28]:

$$p(\theta_r) = \frac{1}{2}\sum_k[k]a_0^k p_k(\cos\theta_r) \tag{12}$$

where the a_0^k coefficients (polarization parameters) are given by $a_0^k = \langle P_k(\cos\theta_r) \rangle$ with the angular brackets stand for an average over all the reactive trajectories. In this paper, $p(\theta_r)$ is expended up to k=18, which shows good convergence.

The dihedral angle distribution of the k - k' - j' three-vector-correlation is characterized by angle ϕ_r [28,30]. It has been shown that the distribution of dihedral angle ϕ_r may be expanded as a Fourier series:

$$p(\phi_r) = \frac{1}{2\pi}[1 + \sum_{neven \geq 2}a_n\cos(n\phi_r) + \sum_{nodd \geq 1}b_n\sin(n\phi_r)] \tag{13}$$

with $a_n = 2\langle\cos(n\phi_r)\rangle$ and $b_n = 2\langle\sin(n\phi_r)\rangle$. In this computation, $p(\phi_r)$ is expanded to n=24, which shows good convergence.

The joint probability density function of angles θ_r and ϕ_r, which define the direction of j', can be written [31] as:

$$p(\theta_r,\phi_r) = \frac{1}{4\pi}\sum_{kq}[k]a_q^k C_{kq}(\theta_r,\phi_r)^* = \frac{1}{4\pi}\sum_k\sum_{q\geq0}[a_{q\pm}^k\cos(q\phi_r) - a_{q\mp}^k i\sin(q\phi_r)]C_{kq}(\theta_r,0) \tag{14}$$

The polarization parameter a_q^k is evaluated as:

$$a_{q\pm}^k = 2\langle C_{k|q|}(\theta_r,0)\cos(q\phi_r)\rangle \qquad\qquad k \text{ is even,} \tag{15}$$

$$a_{q\mp}^k = 2i\langle C_{k|q|}(\theta_r,0)\sin(q\phi_r)\rangle \qquad\qquad k \text{ is odd.} \tag{16}$$

In the calculation, $p(\theta_r,\phi_r)$ is expanded up to k=7, which is sufficient for good convergence.

3.2. Potential energy surface

The extended-London-Eyring-Polanyi-Sato (LEPS) potential energy surface (PES) is applied in our calculation [32]:

$$U(R_1, R_2, R_3,) = Q_1 + Q_2 + Q_3 - \left\{ \frac{1}{2}[(J_1 - J_2) + (J_2 - J_3) + (J_3 - J_1)] \right\}^{1/2} \tag{17}$$

where $Q_i = (^1E_i + {}^3E_i)/2$, $J_i = (^1E_i - {}^3E_i)/2$. ^1E_i is defined as the diatomic Morse potential function, and ^3E_i stands for the anti-Morse function:

$$^1E_i = {}^1D_i \left(\{1 - \exp[-\beta_i(\gamma - \gamma_0)]\}^2 - 1 \right), \tag{18}$$

$$^3E_i = {}^3D_i \left(\{1 + \exp[-\beta_i(\gamma - \gamma_0)]\}^2 - 1 \right). \tag{19}$$

where $^3D_i = {}^1D_i(1 - S_i)/2(1 + S_i)$ and S_i is an adjustable parameter. For the reaction of $A + BC \rightarrow AB + C$, the subscript i = 1, 2, 3 indicate AB, BC and CA, respectively.

The experimental results and the *ab initio* calculations of the $O + CH_4 \rightarrow OH + CH_3$ reaction show that the minimal barrier occurs at a collinear configuration. The alkyl radical does not possess significant internal excitation. So in this paper, the CH_4 is treated as a $H\text{-}CH_3$ pseudo-diatom for approximation. The classical Hamilton equations are integrated numerically for motion in three dimensions. Trajectories are initiated with the CH_4 molecule in v=0 and j=0 levels and the collision energy is 0.65 eV. 100,000 trajectories are sampled, and the integration step size in the trajectories is chosen to be 0.1 fs for the stability of the calculation results. The parameters of extended-LEPS PESs are presented in Table 1 [33]. All the calculations performed here were done under adiabatic approximation.

Table 1. The PES parameters for the $O + CH_4 \rightarrow OH + CH_3$ reaction.

Parameter	O-H	H-CH$_3$	O-CH$_3$
β_e (Å^{-1})[a]	2.294	1.83	1.96
D_e(kJ/mol)[a]	445.34	447.26	384.35
r_e[a]	0.9706	1.093	1.44
Sato C[a]	0.30	0.20	-0.15
Sato D[b]	0.70	0.3702	-0.4

[a] Taken from Reference 33.

[b] This work

4. Conclusions

We have presented a quasiclassical trajectory study of the product polarization from the $O + CH_4 \rightarrow OH + CH_3$ reaction on the new LEPS PES by using a new Sato parameter. The differential cross section $(2\pi/\sigma)(d\sigma_{kq}/d\omega_t)$ show that the scattering is predominantly in the backward hemisphere. For the vector correlation, the J_{OH} is aligned in the plane perpendicular to the line of center and the

four PDDCSs give a good explanation about the vector correlation. From the isotope effect for the reactions O + CH$_4$ and O + CD$_4$ we find that there is a backward scattering tendency with the deuterium instead of hydrogen of the *(2π/σ)(dσ$_{00}$/dω$_t$)* distributions. And the angular momentum polarization ($P(\theta_r)$ and $P(\phi_r)$) of OD is much stronger than that of OH.

Acknowledgements

References and Notes

1. Warnatz, J. *Combustion Chemistry*; Springer-Verlag: Berlin, Germany, 1984.
2. Garton, D.J.; Minton, T.K.; Troya, D.; Pascual, R.Z.; Schatz, G.C. Hyperthermal reactions of O(^{3}P) with alkanes: Observations of novel reaction pathways in crossed-beams and theoretical studies. *J. Phys. Chem. A.* **2003**, *107*, 4583-4587.
3. Sutherland, J.W.; Michael, J.V.; Klemm, R.B. Rate constant for the O(^{3}P) + CH$_4$ .fwdarw. OH + CH$_3$ reaction obtained by the flash photolysis-shock tube technique over the temperature range 760 .ltoreq. T .ltoreq. 1760 K. *J. Phys. Chem.* **1986**, *90*, 5941-5945.
4. Cohen, N.; Westberg, K.R. Chemical kinetic data sheets for high-temperature reactions. part II. *J. Phys. Chem. Ref. Data.* **1991**, *20*, 1211-1311.
5. Suzuki, T.; Hirota, E. Vibrational distribution of CH$_3$ produced by the reaction of O(^{1}D$_2$) atom with CH$_4$. *J. Chem. Phys.* **1993**, *98*, 2387-2398.
6. Sweeney, G.M.; Watson, A.; McKendrick, K.G. Rotational and spin-orbit effects in the dynamics of O(^{3}P$_j$) + hydrocarbon reactions. I. Experimental results. *J. Chem. Phys.* **1997**, *106*, 9172-9182.
7. Ausfelder, F.; McKendrick, K.G. The dynamics of reactions of O(^{3}P) atoms with saturated hydrocarbons and related compounds. *Prog. Reac. Kinet. Mech.* **2000**, *25*, 299-370.
8. Gonzalez, M.; Hernando, J.; Millan, J.; Sayos, R. *Ab initio* ground potential energy surface, VTST and QCT study of the O(^{3}P) + CH$_4$($X\,^1A_1$) → OH(X2Π) + CH3(X2A2″) reaction. *J. Chem. Phys.* **1999**, *110*, 7326-7338.
9. Espinosa-Garcia, J.; Garcia-Bernaldez, J.C. Analytical potential energy surface for the CH$_4$ + O(^{3}P) → CH$_3$ + OH reaction. Thermal rate constants and kinetic isotope effects. *Phys. Chem. Chem. Phys.* **2000**, *2*, 2345-2352.
10. Huarte-Larranaga, F.; Manthe, U. Accurate quantum dynamics of a combustion reaction: Thermal rate constants of O(^{3}P) + CH$_4$(X $^1A_1$) → OH(X2Π) + CH3(X2A2″). *J. Chem. Phys.* **2002**, *117*, 4635-4638.
11. Dutton, N.J.; Fletcher, I.W.; Whitehead, J.C. Laser-induced fluorescence determination of the internal state distributions of OH($X\,^2$Π) produced in molecular beam reactions of O(^{3}P) with some cyclic hydrocarbons. *Mol. Phys.* **1984**, *52*, 475-483.

12. Corchado, J.C.; Espinosa-Garcia, J.; Roberto-Neto, O.; Chuang, Y.Y.; Truhlar, D.G. Dual-level direct dynamics calculations of the reaction rates for a jahn−teller reaction: Hydrogen abstraction from CH_4 or CD_4 by $O(^3P)$. *J. Phys. Chem. A.* **1998**, *102*, 4899-4910.

13. Troya, D.; Pascual, R.Z.; Schatz, G.C. Theoretical studies of the $O(^3P)$ + Methane reaction. *J. Phys. Chem. A.* **2003**, *107*, 10497-10506.

14. Sayos, R.; Hernando, J.; Puyuelo, M.P.; Enriquez, P.A.; Gonzalez, M. Collision energy effects on the dynamics of the reaction $O(^3P)$ + $CH_4(X1A1)$ → $OH(X2\Pi)$ + $CH_3(X2A2'')$. *Chem. Phys. Lett.* **2001**, *341*, 608-618.

15. Troya, D.; Schatz, G.C.; Garton, D.J.; Brunsvold, A.L.; Minton, T.K. Crossed beams and theoretical studies of the $O(^3P)$ + CH_4→ H + OCH_3 reaction excitation function. *J. Chem. Phys.* **2004**, *120*, 731-739.

16. Clary, D.C. Quantum dynamics of the $O(^3P)$ + CH_4 → CH_3 + OH reaction. *Phys. Chem. Chem. Phys.* **1999**, *1*, 1173-1180.

17. Palma, J.; Clary, D.C. The effect of the symmetric and asymmetric stretching vibrations of CH_4 on the $O(^3P)$ + CH_4 → OH + CH_3 reaction. *Phys. Chem. Chem. Phys.* **2000**, *2*, 4105-4114.

18. Palma, J.; Echave, J.; Clary, D.C. The effect of the symmetric and asymmetric stretching vibrations on the CH_3D + $O(^3P)$ → CH_3 + OD reaction. *Chem. Phys. Lett.* **2000**, *363*, 529-533.

19. Wang, M.L; Li, Y.L.; Zhang, J.Z. Application of semirigid vibrating rotor target model to the reaction of $O(^3P)$ + CH_4 → CH_3 + OH. *J. Phys. Chem. A.* **2001**, *105*, 2530-2534.

20. Troya, D.; García-Molina, E. Quasiclassical trajectory study of the $O(^3P)$ + CH_4 → OH + CH_3 reaction with a specific reaction parameters semiempirical hamiltonian. *J. Phys. Chem. A.* **2005**, *109*, 3015-3023.

21. Yan, T.Y.; Hase, W.L.; Doubleday, C. Energetics, transition states, and intrinsic reaction coordinates for reactions associated with $O(^3P)$ processing of hydrocarbon materials. *J. Chem. Phys.* **2004**, *120*, 9253-9265.

22. Orr-Ewing, A.J.; Simpson, W.R.; Rakitzis, T.P.; Kandel, S.A.; Zare, R.N. Scattering-angle resolved product rotational alignment for the reaction of Cl with vibrationally excited methane. *J. Chem. Phys.* **1997**, *106*, 5961-5971.

23. Simpson, W.R.; Rakitzis, T.P.; Kandel, S.A.; Lev-On, T.; Zare, R.N.; Picturing the transition-state region and understanding vibrational enhancement for the Cl + CH_4 → HCl + CH_3 reaction *J. Phys. Chem.* **1996**, *100*, 7938-7947.

24. Kandel, S.A.; Rakitzis, T.P.; Lev-On, T.; Zare, R.N. Dynamics for the Cl + C_2H_6 → HCl + C_2H_5 reaction examined through state-specific angular distributions. *J. Chem. Phys.* **1996**, *105*, 7550-7557.

25. Kandel, S.A.; Rakitzis, T.P.; Lev-On, T.; Zare, R.N. Dynamical effects of reagent vibrational excitation in the Cl + $C_2H_6(v_5 = 1)$ → HCl + C_2H_5 reaction. *Chem. phys. Lett.* **1997**, *265*, 121-128.

26. Orr-Ewing, A.J.; Zare, R.N. Orientation and alignment of reaction products *Annu. Rev. Phys. Chem.* **1994**, *45*, 315-366.

27. Zhang, B.l.; Liu, K. How active is the bend excitation of methane in the reaction with $O(^3P)$? *J. Phys. Chem. A.* **2005**, *109*, 6791-6795.

28. Aoiz, F.J.; Brouard, M.; Enriquez, P.A. Product rotational polarization in photon-initiated bimolecular reactions. *J. Chem. Phys.* **1996**, *105*, 4964-4982.

29. Brouard, M.; Lambert, H.M.; Rayner, S.P.; Simpson, J.P. Product state resolved stereodynamics of the reaction H(^{2}S) + CO$_2$ OH(X$^2\Pi_{3/2}$; v = 0, N = 5) CO($^1\Sigma^+$). *Mol. Phys.* **1996**, *89*, 403-423.

30. Aoiz, F.J.; Brouard, M.; Herrero, V.J.; Rábanos, V.S.; Stark, K. Product rotational polarization. The stereodynamics of the F + H$_2$ reaction. *Chem. Phys. Lett*. **1997**, *264*, 487-494.

31. Alexander, A.J.; Aoiz, F.J.; Bañareas, L.; Brouard, M.; Short, J.; Simons, J.P. Stereodynamics of the reaction O(^{1}D$_2$) + H$_2$(v=0) → OH(X$^2\Pi_i$;v'=0,N',f) + H: State-resolved linear and rotational angular momentum distributions. *J. Phys. Chem. A*. **1997**, *101*, 7544-7557.

32. Han, K.L.; He, D.G.; Lou, N.Q. Effect of location of energy barrier on the product alignment of reaction *A* + *BC*. *J. Chem. Phys*. **1996**, *105*, 8699-8704.

33. Xu, L.J.; Yan, J.M.; Zhen, Z.; Kong, F.A.; Zhu, Q.H. QCT for the reaction of CH$_4$ ＋ O(^{3}P) → CH$_3$ ＋ OH. *Acta. Phys. Chim. Sinica* **1997**, *13*, 999-1004.

34. Li, R.J.; Han, K.L.; Li, F.E.; Lu, R.C.; He, G.Z.; Lou, N.Q. Rotational alignment of product molecules from the reactions Sr$^+$ CH$_3$Br, C$_2$H$_5$Br, *n*-C$_3$H$_7$Br, *i*-C$_3$H$_7$Br by means of PLIF. *Chem. Phys. Lett.* **1994**, *220*, 281-285.

35. Wang, M.L.; Han, K.L.; He, G.Z. Product rotational polarization in the photoinitiated bimolecular reaction *A* + *BC*→ *AB* + *C* on attractive, mixed and repulsive surfaces. *J. Chem. Phys.* **1998**, *109*, 5446-5454.

36. Wang, M.L.; Han, K.L.; He, G.Z.; Lou, N.Q. Product rotational polarization in photo-initiated bimolecular reactions A + BC: Dependence on the character of the potential energy surface for different mass combinations. *J. Phys. Chem. A*. **1998**, *102*, 10204-10210.

37. Sweeney, G.M.; Watson, A.; McKendrick, K.G. Rotational and spin-orbit effects in the dynamics of O(^3P_j) + Hydrocarbon reactions. II. Models for spin-orbit propensities. *J. Chem. Phys.* **1997**, *106*, 9182-9189.